Contents lists available at Science-Gate

International Journal of Advanced and Applied Sciences

Journal homepage: http://www.science-gate.com/IJAAS.html

Development of an automated multi-thresholding technique for identification of different materials types and concentration using CT scans

Lay Yean Ng [1,*], Moayyad Al Ssabbagh [2], Abd Aziz Tajuddin [1,2], Ibrahim Lutfi Shuaib [1], Rafidah Zainon [1]

[1]*Advanced Medical and Dental Institute, Universiti Sains Malaysia, Pulau Pinang, Malaysia*
[2]*School of Physics, Universiti Sains Malaysia, Pulau Pinang, Malaysia*

ARTICLE INFO

Article history:
Received 17 January 2017
Received in revised form
27 November 2017
Accepted 18 December 2017

Keywords:
Dual-energy
Single-energy
Algorithm
Thresholding
Concentrations

ABSTRACT

The aim of this study is to evaluate the efficacy of a new automated quantification technique in differentiating different types of materials using the single-energy and dual-energy computed tomography (CT). Five different concentrations of calcium chloride, and two different concentrations of iron (III) nitrate and sunflower oil were used. The eight solutions were placed into a PMMA container, which was filled with water and scanned using a single-source dual energy CT that is capable of producing single and dual-energy images. Five energies (70, 80,100, 20 and 140 kVp) were applied to produce the single-energy images, while only two energies with high (140 Kvp) and low voltages (80 kVp) were used to produce the fused CT images. The pitch and slice thickness selected were 0.6 mm and 1 mm respectively. The developed image processing software was used to evaluate the CT numbers of each type of solution. The results were compared with the Weasis software v1.2.7 and Somaris7/Syngro CT2012B to verify the new algorithm. The developed automatic multi-thresholding algorithm can differentiate solutions with high concentration from different type of materials. The mean percentage differences of CT numbers obtained from new algorithm, Weasis software and Syngro software show no significant difference. The developed multi-thresholding algorithm was unable to distinguish between low concentration solutions. However, it had the ability to detect the solutions with high concentration from each material. The developed image processing software based on multi-thresholding method showed promising results to detect different type of materials with various concentrations, which can aid in detecting different types of plaques in coronary heart disease.

© 2017 The Authors. Published by IASE. This is an open access article under the CC BY-NC-ND license (http://creativecommons.org/licenses/by-nc-nd/4.0/).

1. Introduction

The dual energy CT that used two separate x-ray sources give high-quality images of the coronary arteries, which reconstructs the output images from half-rotation at an angle of 90°. Using this technique, the high-quality imaging enhanced the recognition of non-invasive plaque, where the CT numbers can be varied for different types of plaques (Henzler et al., 2011; Motoyama et al., 2009). It has been reported in many studies that the CT numbers, which are measured in Hounsfield Unit (HU) can be used to recognize different human tissue, such as lipid-rich ones. On the other hand, lipid-rich tissues caught attention in non-calcified lesions since it increases the possibility of cardiovascular disease.

According to several studies, it was found that using the HU allowed characterization of these lipid-rich lesions using the new multi-detector CT scans (Kristanto et al., 2013). Apart from that, high numbers of multi-detector CTs showed a better demonstration of characterizing the calcified plaques. The calcium in the calcified lesions has high attenuation properties, which can be detected clearly in CT images. Thus, the calcium score encourages the methods to detect such cardiovascular disorders. In CT angiography, the use of contrasts in coronary diseases is considered essential nowadays. But not in evaluating the calcification in the coronary artery using the CT scans, whereas the HU of these calcifications are very high and can easily be detected (Kristanto et al., 2012).

* Corresponding Author.
Email Address: ngly2008@gmail.com (L. Y. Ng)
https://doi.org/10.21833/ijaas.2018.03.001
2313-626X/© 2017 The Authors. Published by IASE.
This is an open access article under the CC BY-NC-ND license (http://creativecommons.org/licenses/by-nc-nd/4.0/)

In a study done by Hong et al. (2003), the mass and the calcium score of the coronary artery were evaluated from two CT scans at 130 HU and 90 HU. Their algorithm shows that measuring the mass of the calcium is more accurate in coronary calcium quantification rather than measuring its volume. Accurate quantifications of calcium in each calcified plaque may require that the threshold is set individually, depending on the calcium density.

Agatston scoring system is software developed by Agatston to characterize the calcified plaque mentioned in many studies. The software can automatically recognize and measure the calcified plaques at 130 HU and make measurements as small as the plaque size (Carr et al., 2005). The calcified plaque identified by the Agatston score is multiplied by the higher attenuation of the calcified tissue, where 130 HU is used as a threshold to classify the calcified and non-calcified lesions. It is common to use this scoring method in computed tomography (CT) to evaluate the coronary atherosclerotic plaques (Hong et al., 2003). Two methods are clinically used to evaluate the calcification; the volume score and Agatston score. The Agatston score considers the threshold larger than 130 HU at 120 kVp as a reference to characterize the calcified tissue (Yamak, 2013).

In addition, using the DECT will significantly reduce the artefacts. This improvement reduces the artifacts in the produced images, such as the beam hardening that appears clearly in single-source CT. It was found that the measured CT numbers in SSCT are higher than the DECT with the value of 35 HU (Henzler et al., 2011).

The computer-aided diagnosis (CAD) could be used to improve the process of handling the cases automatically to avoid data overload and the human errors. The use of high-quality computers in this technology will attain rapid and reliable results. In addition, CAD can provide the patients with information remotely which will help hasten support to those who need rapid medical intervention. Until now, there is no general algorithm to evaluate every image in the medical field, particularly in automatic segmentation. The results from such algorithms may be influenced by non-uniform intensity, artifacts and the nearest attenuation values of the soft tissue, which is considered as the most disturbing problem in the evaluation of medical images (Sharma and Arggarwal, 2010).

In medical imaging, the segmentation methods rely on the part under examination, imaging modality and what it will be used for. Dividing the image into different areas according to colour, brightness and contrast will subdivide the objects in the image. This process called segmentation. The importance of segmentation in medical imaging will enhance body structure studies, recognize the tumour location and its size during the diagnosis and assist in calculations of radiotherapy treatment planning. In radiotherapy planning, the computed tomography (CT) imaging is used widely, in radiotherapy planning, where the exact segmentation of the output images is the major step to contour the examined structure of the patient's body (Sharma and Aggarwal, 2010).

The most convenient and commonly used method in segmentation is using the thresholding method based on the image histogram (Demirkaya et al., 2008). Image thresholding is the fastest and easiest method for image segmentation. This method depends on converting the image into a binary image, which has limited applications. This method can achieve outstanding results in some applications but poor in the others (Rais et al., 2004).

One of the two methods of determining the threshold levels is the global thresholding method while the other utilizes local thresholding. The global thresholding relies on many ways, such as using the virtual observation of the histogram modes to differentiate between them, or using the trial and error method until finding the suitable threshold according to observer preferences. The local thresholding method uses multiple thresholds for multiple window regions (Gonzales et al., 2006; Rais et al., 2004).

Other than the thresholding method, the most used segmentation methods are the region-based segmentation and the edge-based segmentation. The region-based method uses region merging and region splitting where selected regions are split and merged. This method is inadequate, where the regions of the images may become under or over the segmentation.

In contrast, the edge-based method depends on the grey level, colour and other variables which are separated into different regions. Moreover, it also affected by the noise and non-smooth or fake edges in the image (Kamdi and Krishna, 2012; Sharma and Arggarwal, 2010). If the properties were similar and the edge outline was clearly visible, this could provide good segmentation results.

2. Materials and methods

Five different concentrations of calcium chloride anhydrous grade of analytical reagents (Grade AR) (20.98, 70.89, 152.10, 204.93 and 356.75 mg/ml) and two different concentration of Iron (III) nitrate (51.71 mg/ml and 96.85 mg/ml) were used to fill seven PMMA tubes. One more tube was filled with sunflower oil. The tubes were placed then placed in a PMMA container with a diameter of 10 cm and a height of 10 cm as shown in Fig. 1.

The container was filled with water and the materials with different concentrations were scanned using a single-source dual-energy CT (Somatom Definition; Siemens AG, Germany) that was capable of producing single-energy and dual-energy images with different applied voltages. Five voltages were applied (70, 80, 100, 120 and 140 kVp) to produce the single-energy images while only low energy (80 kVp) and high energy (140 kVp) were applied to produce the fused images from the dual energy mode. The automatic current modulation CARE DOSE 4D was used for both

scanning modes, while the slice width was set to 1 mm.

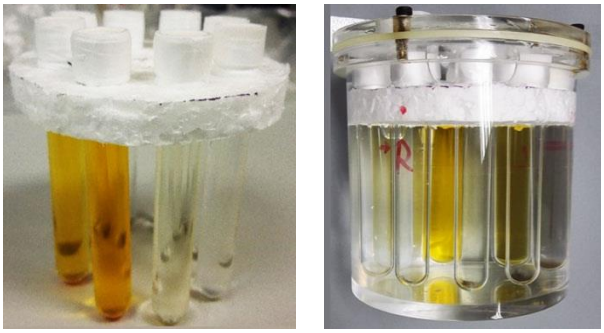

Fig. 1: The PMMA tubes filled with the materials and inserted into the PMMA phantom

The output DICOM images from DECT and SECT were analysed using the Weasis Medical Viewer v.1.2.7, developed by Nicolas Roduit (Gutman et al., 2014). The region of interest (ROI) was selected for each material and the CT numbers were measured as illustrated in Fig. 2.

The mean and the standard deviation of the CT numbers of each material were then calculated for both scanning modes. Somaris7/Syngro CT 2012a built by Siemens was used to evaluate the same images. The same area of ROI with the same location on each material was applied to each CT image and the CT numbers were measured as shown in Fig. 3.

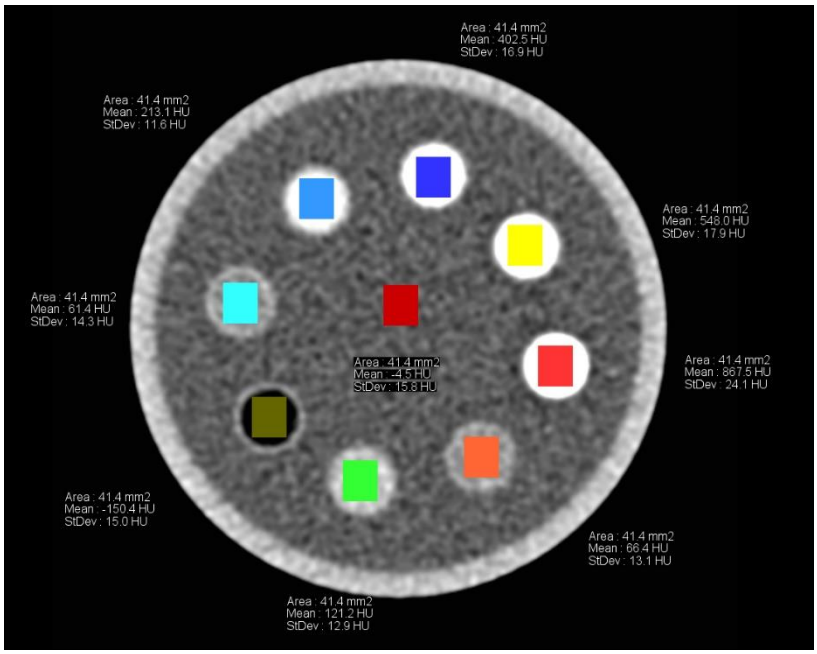

Fig. 2: CT numbers of each material from Weasis software at a tube voltage of 80 kVp

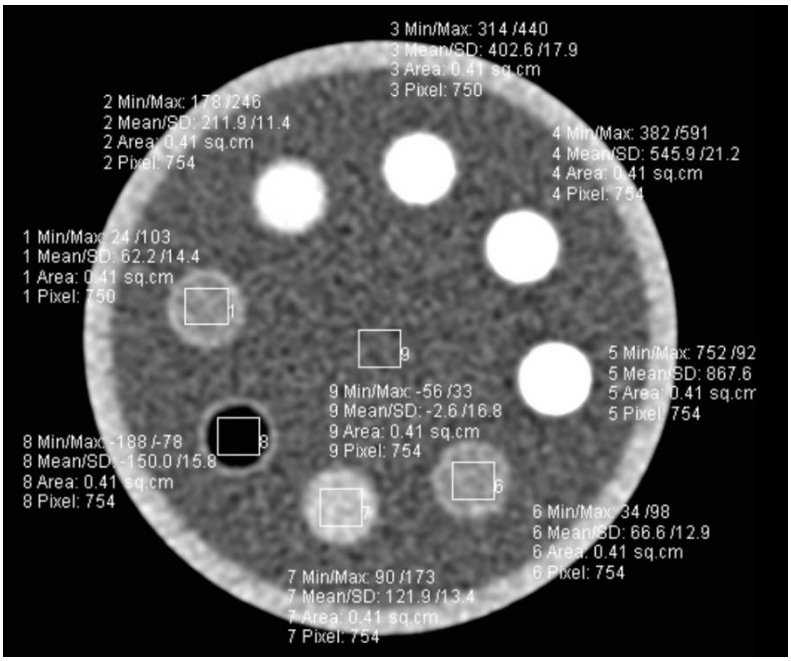

Fig. 3: Evaluated CT numbers using Syngro for each material at a tube voltage of 80 kVp

The same images were evaluated using the new algorithm developed on MATLAB® software v. R2014a. The same area of ROI with the same location on each material was applied and the CT

numbers were computed and stored in an array format. The results from the Weasis and the new system were compared and the percentage difference was calculated.

The CT numbers were evaluated where the minimum and maximum threshold for each material concentration were set based on the mean CT numbers and the standard deviations obtained from the new algorithm. The same images were used to test the algorithm.

3. Results and discussion

The CT images in the DICOM format were imported into the automatic system and the algorithm was applied. The same area and location were selected for each material and the pixel value of each ROI was evaluated. To calculate the CT numbers of each selected ROI for each material with different solution concentrations, Eq. 1 was used.

$$CT\ numbers = Pix \times RS + RI \quad (1)$$

Where Pix is the pixel value which contains the information of the DICOM images that will be used to multiply with the RescaleSlope (RS) and RescaleIntercept (RI) in order to convert the results to Hounsfield units (HU). It was noticed that the Rescale Slope and Rescale Intercept could have different values when used in different algorithms (Kamath et al., 2011).

After the images were converted from the pixel value to CT number for each the ROI from each material, the results were stored into an array format for all images. The information of each array will be used to calculate the mean of the CT numbers and the standard deviation for each ROI.

Due to the DICOM images that were imported to the new algorithm is in pixels and not a length-based unit, Eq. 2 was applied to convert the pixel value to mm scale in order to know the area of ROI. This value will be used to select the same area of ROI using two other kinds of software widely used in analysing CT images to verify the conversion of CT numbers obtained from our algorithm.

$$Area\ of\ ROI\ (mm^2) = (PL \times PS) \times (PW \times PS) \quad (2)$$

Where the pixel length and pixel width referred to the length and the width of the rectangular shape of the ROI. The pixel spacing is the distance between the two pixels in a row and column in the unit of millimetre (mm). Normally, the distance between 2 pixels was measured from the centre.

The CT numbers evaluated from the developed software were compared with the CT numbers obtained from Weasis and Syngro to ensure the conversion was done correctly before moving to the next step as illustrated in the flowchart (Fig. 4). The Weasis and Syngro software were selected for the verification process. The same slice number and ROI size and location were set carefully when obtaining the CT number (mean) and standard deviation with Weasis and Syngro. The mean of the CT numbers and the standard deviation were calculated for each material at all energy levels in both single energy and dual energy images.

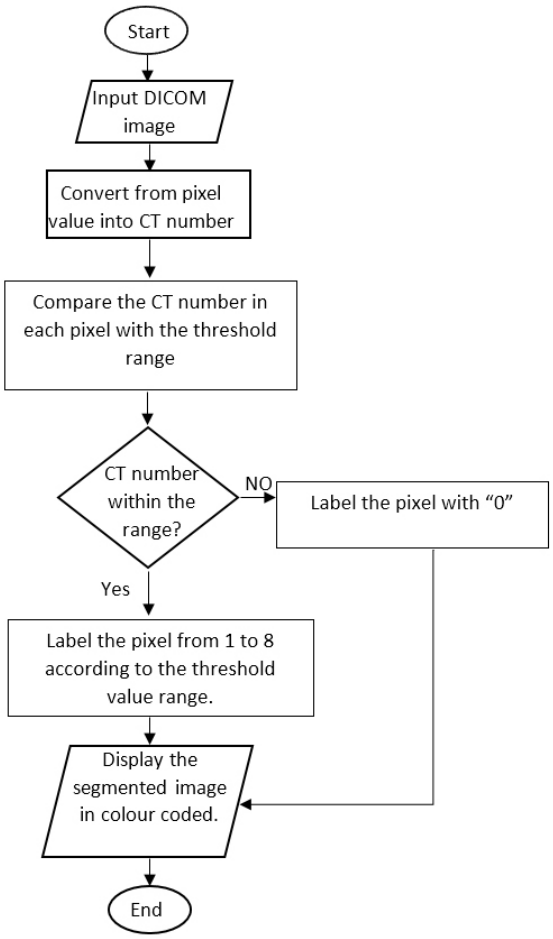

Fig. 4: Flow chart of the process flow for the image segmentation

The ROI with an area of 0.41 cm^2 was applied on the CT images from the single-energy mode for each material concentration, while the area of 0.37 cm^2 was used in the dual-energy mode. The same ROI was applied in the three software (The newly developed system, Weasis and Syngro) that used in this study for both modes.

As seen from the Figs. 5 and 6, the results obtained from Weasis, Syngro and the new algorithm were almost overlapped, where the evaluated CT numbers of each solution concentration showed similar values from each software at different applied voltage from both the single-energy and dual-energy techniques.

The mean percentage difference of the evaluated CT numbers from the single-energy mode between the new system and Weasis was -0.012 % whereas it was 0.064 % between the new system and the Syngro, while it was 0.076% between Weasis and Syngro. All the means values show insignificant differences. In contrast, the mean percentage differences also showed no significant values from the dual-energy mode, where the values were 0.135

%, -0.427% and -0.563% respectively for the same comparison done in single-energy mode.

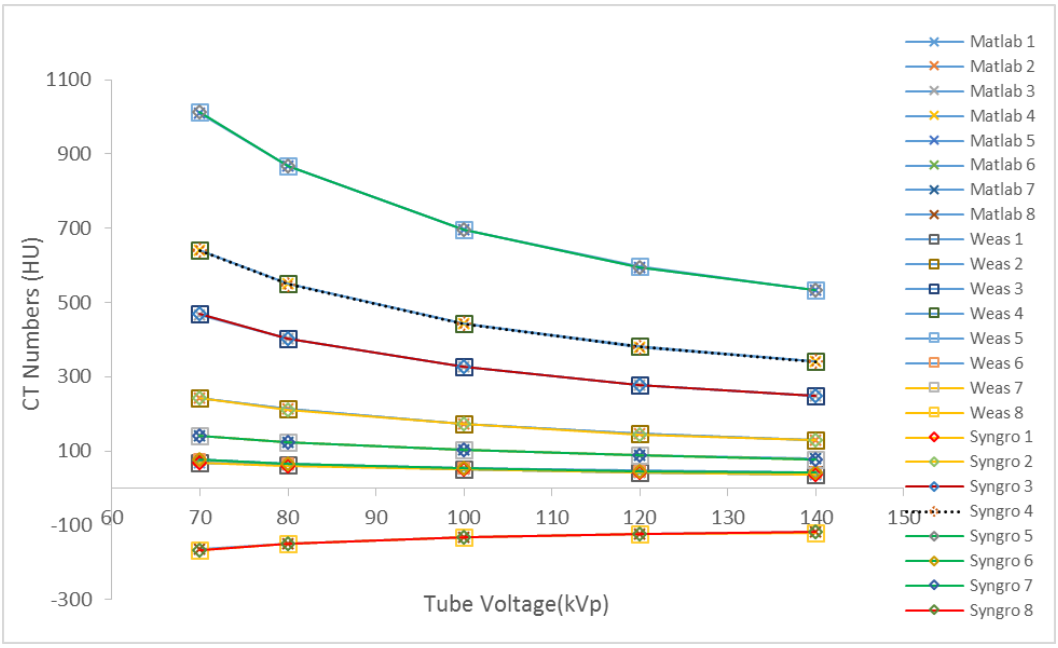

Fig. 5: The obtained CT number from the new algorithm compared with the CT numbers obtained from Weasis and Syngro at different energy levels in SECT

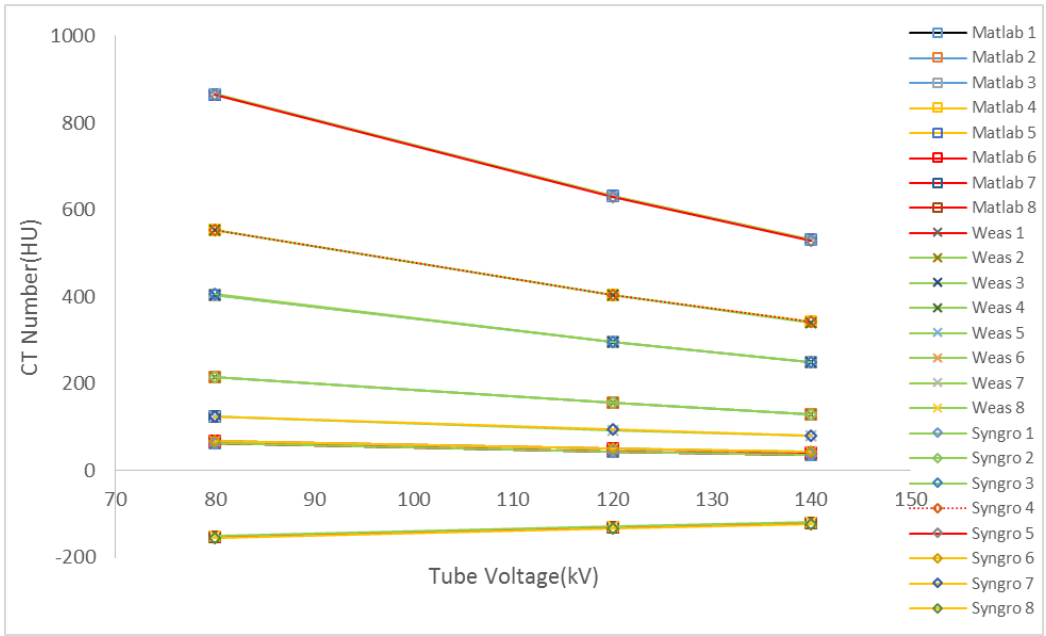

Fig. 6: The obtained CT numbers from the new algorithm at different energy levels in DECT compared with Weasis and Syngro

In our algorithm, we used the multi-thresholding method to perform the segmentation. The threshold for each material concentration was set according to the measured CT numbers from Weasis, Syngro software and the newly developed system for both scanning modes. The new algorithm analysed the CT images, where every pixel value was compared with the threshold for each material with different concentration. The algorithm was tested with the CT images from the single-energy at 120 kV and from the fused image from the dual-energy modes as shown in Fig. 7 and Fig. 8.

From the Figs. 7 and 8, the system was unable to distinguish between the solutions with a low concentration of calcium chloride (20.977 mg/ml) and iron (III) nitrate (51.706 mg/ml). The CT numbers for these low concentrations were between 30 HU to 60 HU for the calcium chloride (20.977 mg/ml) and also iron (III) nitrate (51.706 mg/ml), at the same energy (120 kV).

Despite the different types of materials, the CT numbers of these materials at these concentrations were very close and the system was unable to distinguish between them. In contrast, the algorithm showed an astonishing ability to detect the solutions with high concentrations in each material. The measured CT numbers for these high concentrations

can be detected very easily by the new automatic technique.

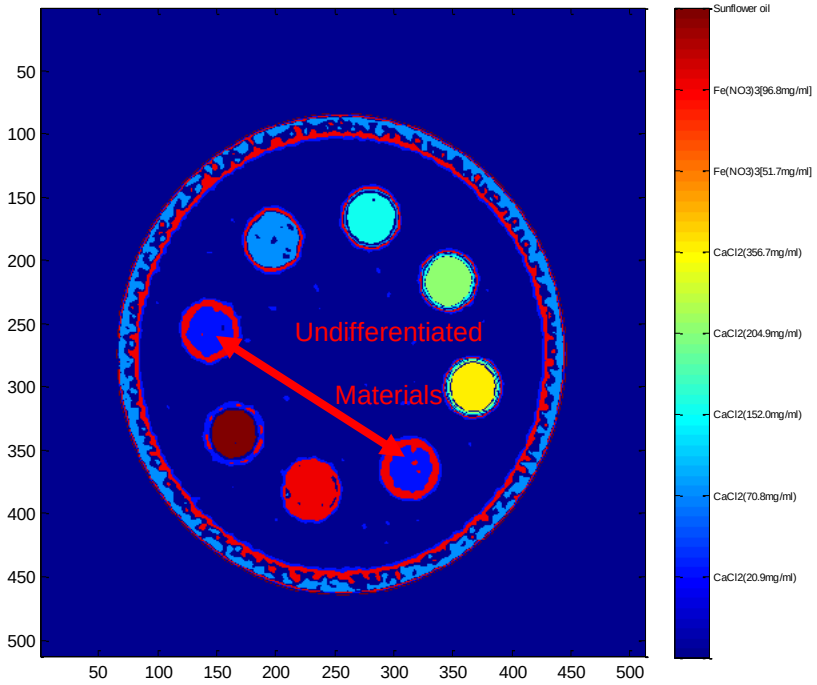

Fig. 7: The output images after applying the algorithm on the fused images from DECT

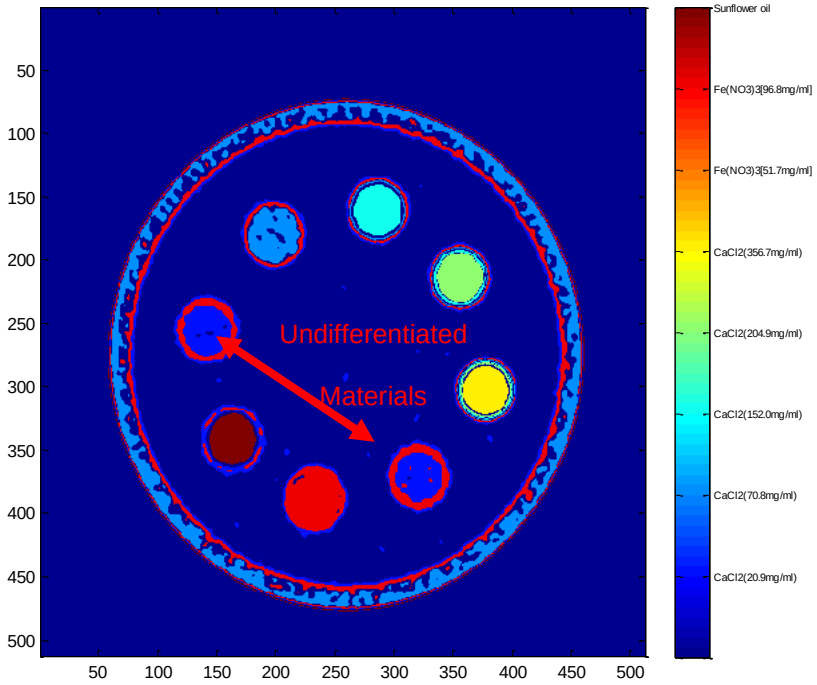

Fig. 8: The output images after applying the algorithm from SECT at 120 kVp to differentiate between different material concentrations

4. Conclusion

Two different DICOM images analyzing software for CT images (Weasis and Syngro) were used to verify the automatic algorithm, which is capable of measuring the correct CT numbers from both single-energy and dual-energy scanning modes.

The new algorithm based on a multi-thresholding method shows promising results to detect different types of materials with various concentrations, which can help detect different types of plaques in blood vessels. However, further investigation is required to improve the algorithm in order to distinguish between the materials that have very

close CT numbers. Other techniques need to be collaborated with the multi-thresholding method in order to further differentiate materials in this situation. Material decomposition is one of the techniques which may help to distinguish these anomalies (Liu et al., 2009).

References

Carr JJ, Nelson JC, Wong ND, McNitt-Gray M, Arad Y, Jacobs JDR, Sidney S, Bild DE, Williams OD, and Detrano RC (2005). Calcified coronary artery plaque measurement with cardiac CT in population-based studies: Standardized protocol of multi-ethnic study of atherosclerosis (MESA) and coronary artery risk development in young adults (CARDIA) study. Radiology, 234(1): 35-43.

Demirkaya, O, M H Asyali, and P K Sahoo (2008). Image processing with MATLAB: Applications in medicine and biology. CRC Press, Ney York, USA.

Gonzales RC, Woods RE, and Eddins SL (2006). Digital image processing using MATLAB [Russian translation]. Google Scholar, Tekhnosfera, Moscow: 206-253.

Gutman DA, Dunn JWD, Cobb J, Stoner RM, Kalpathy-Cramer J, and Erickson B (2014). Web based tools for visualizing imaging data and development of XNATView, a zero footprint image viewer. Frontiers in Neuroinformatics, 8: Article 53. https://doi.org/10.3389/fninf.2014.00053

Henzler T, Porubsky S, Kayed H, Harder N, Krissak UR, Meyer M, Sueselbeck T, Marx A, Michaely H, Schoepf UJ, and Schoenberg SO (2011). Attenuation-based characterization of coronary atherosclerotic plaque: Comparison of dual source and dual energy CT with single-source CT and histopathology. European Journal of Radiology, 80(1): 54-59.

Hong C, Bae KT, and Pilgram TK (2003). Coronary artery calcium: Accuracy and reproducibility of measurements with Multi–Detector Row CT—assessment of effects of different thresholds and quantification methods. Radiology, 227(3): 795-801.

Kamath S, Song W, Chvetsov A, Ozawa S, Lu H, Samant S, Liu C, Li JG, and Palta JR (2011). An image quality comparison study between XVI and OBI CBCT systems. Journal of Applied Clinical Medical Physics, 12(2): 376-390.

Kamdi S and Krishna RK (2012). Image segmentation and region growing Aalgorithm. International Journal of Computer Technology and Electronics Engineering 2(1): 103–107.

Kristanto W, Van Ooijen PM, Groen JM, Vliegenthart R, and Oudkerk M (2012). Small calcified coronary atherosclerotic plaque simulation model: Minimal size and attenuation detectable by 64-MDCT and MicroCT. The International Journal of Cardiovascular Imaging, 28(4): 843-853.

Kristanto W, Van Ooijen PM, Jansen-van der WMC, Vliegenthart R, and Oudkerk M (2013). A meta-analysis and hierarchical classification of HU-based atherosclerotic plaque characterization criteria. PLoS ONE, 8(9): 1–13.

Liu X, Yu L, Primak AN, and McCollough CH (2009). Quantitative imaging of element composition and mass fraction using dual-energy CT: Three-material decomposition. Medical Physics, 36(5): 1602-1609.

Motoyama S, Sarai M, Harigaya H, Anno H, Inoue K, Hara T, Naruse H, Ishii J, Hishida H, Wong ND, and Virmani R (2009). Computed tomographic angiography characteristics of atherosclerotic plaques subsequently resulting in acute coronary syndrome. Journal of the American College of Cardiology, 54(1): 49-57.

Rais NB, Hanif MS, and Taj IA (2004). Adaptive thresholding technique for document image analysis. In the 8th International Multitopic Conference of INMIC, IEEE: 61-66. https://doi.org/10.1109/INMIC.2004.1492847

Sharma N and Aggarwal LM (2010). Automated medical image segmentation techniques. Journal of Medical Physics, 35(1): 3–14.

Yamak D (2013). Characterization of coronary atherosclerotic plaques by dual energy computed. Ph.D. Dissertation, Arizona State University, Arizona, USA.